

Large dynamical magnetic effective charges in the Jahn-Teller KCoF₃

Bogdan Guster,¹ Maxime Braun,^{1,2} and Eric Bousquet¹

¹*Physique Théorique des Matériaux, QMAT, CESAM, Université de Liège, B-4000 Sart-Tilman, Belgium*

²*Univ. Lille, CNRS, Centrale Lille, ENSCL, Univ. Artois, UMR 8181-UCCS-Unité de Catalyse et Chimie du Solide, F-59000 Lille, France*

We compute from density functional theory calculations the dynamical magnetic effective charges of the Jahn-Teller ground state of KCoF₃ and we unexpectedly obtain the largest up-to-date values reported in real materials (close to $200 \times 10^{-2} \mu_B/\text{\AA}$). We determine that those large values are due to both spin and orbital contributions, as expected from the presence of unquenched Co-d orbital magnetic moment, even though we show that the Co dynamical magnetic effective charges values are surprisingly zero by symmetry. Hence, we conclude that even if KCoF₃ is not multiferroic, it is antimagnetoelectric with a compensating but large individual magnetic sublattice magnetoelectric response of 210 ps/m per spin-channel. Our study shows that the dynamical magnetic effective charges might be an important property of magnetic materials beyond the magnetoelectric ones.

Magnetolectrics experienced a vivid comeback in the past 15 years especially due to the intense research brought upon by multiferroic materials [1–4]. Only recently the absence of such a response is explained elegantly based on a *hidden* order stemming from the intrinsic magnetolectric multipole ordering [5–9]. Although the absence of a global magnetolectric response doesn't imply the absence of a local ME. The existence of locally ordered magnetolectric multipoles that overall gives rise to a globally nil response is called antimagnetolectricity. [9] At a theoretical level, the magnetolectric multipoles can be matched with the magnetic response of a crystal upon atomic perturbation, in the form of Dynamical Magnetic Charges (DMCs) [10]. Recently, we have shown the presence of large DMCs in BiCoO₃ and analysed the correspondence with the magnetolectric multipoles counterpart [12]. Even though multiferroic, BiCoO₃ shows an anti-magnetolectric response in its magnetic ground state with contributions arising from both spin and orbital degrees of freedom. [11, 12]. While the spin degree of freedom origin of the magnetic properties of materials is widely explored, its orbital counterpart starts to gain attention somewhat recently and new venues for the orbital degree of freedom exploitation are proposed, bringing upon the field of orbitronics [13] or transistor technologies based on spin-orbit logic in magnetolectric materials [14].

First, let us reassess the importance of the spin and orbital magnetic moments coupled to an electric field. The linear magnetolectric effect, which is the coupling between the electric and magnetic degrees of freedom in materials, can be simply traced from the net magnetization \mathbf{M} (polarization \mathbf{P}) induced by the applied electric (magnetic) field's amplitude:

$$\alpha_{ij} = \mu_0 \left. \frac{\delta M_j}{\delta \mathcal{E}_i} \right|_{\mathcal{H}} = \left. \frac{\delta P_i}{\delta \mathcal{H}_j} \right|_{\mathcal{E}}. \quad (1)$$

From the theoretical standpoint, the second-rank tensor α_{ij} can be decomposed into three contributions: electronic, lattice and strain, $\alpha^{tot} = \alpha^{elec} + \alpha^{latt} + \alpha^{str}$, each

of which arising from the coupling with either the spin, \vec{S} , or the orbital, \vec{L} , degrees of freedom. While the electronic component (α^{elec}) response requires the presence of a spontaneous polarization to be nonzero, it is not the case for the latter two. In fact, lattice-mediated terms can give rise to a significant response in the vicinity of a ferroelectric phase transition [15, 16]. Furthermore, the full magnetolectric response can be strongly enhanced as a results of an unquenched orbital magnetic moment due to a strong lattice-orbital coupling [11, 17, 18]. We remind from a previous work [12] that the lattice-mediated contribution to the magnetolectric tensor takes the following form:

$$\alpha_{ij}^{latt} = \frac{\mu_0}{\Omega} \sum_{n=1}^{N_{IR}} \frac{S_{n,ij}}{\omega_n^2}, \quad (2)$$

where ω_n the phonon *angular* frequencies corresponding to the N_{IR} infrared-active phonon modes, and $S_{n,ij}$ is the magnetolectric mode-oscillator strength tensor, defined as follows:

$$S_{n,ij} = \left(\sum_{\kappa, i'} Z_{\kappa, i' i}^{*m} u_{n, \kappa, i'} \right) \times \left(\sum_{\kappa, j'} Z_{\kappa, j' j}^{*e} u_{n, \kappa, j'} \right), \quad (3)$$

where κ identifies the atom in the unit cell, $u_{n, \kappa, j}$ the normalized eigendisplacement, Z_{κ}^{*e} and Z_{κ}^{*m} the Born effective charge (BEC) and dynamical magnetic effective charge (DMC), respectively, defined as:

$$Z_{\kappa, ij}^{*e} = \Omega \frac{\partial P_i}{\partial \tau_{\kappa, j}} = \frac{\partial^2 E}{\partial \mathcal{E}_i \partial \tau_{\kappa, j}}, \quad (4)$$

i.e., the net polarization along direction i induced by a displacement τ of atom κ along direction j , and

$$Z_{\kappa, ij}^{*m} = \Omega \frac{\partial M_i}{\partial \tau_{\kappa, j}} = \frac{\partial^2 E}{\partial \mathcal{H}_i \partial \tau_{\kappa, j}}, \quad (5)$$

which corresponds to the net magnetization along direction i , induced by a displacement τ of atom κ along direction j [10].

Those DMCs have been used recently to explain the anti-magnetolectric case [9] where the global magneto-lectric response is zero but the local one is not, similarly to antiferromagnetism with non zero atom magnetic moments that are anti-aligned from site to site and giving zero total magnetization [12].

While DMCs were defined through magnetolectric and multiferroic materials [10, 12, 16], in this work we show that large DMC can exist in non-functional materials. We study the anti-magnetolectric effect in the antiferromagnetically ordered KCoF_3 perovskite crystal in the presence of a Jahn-Teller instability by means of *ab initio* calculations.

Our density functional theory (DFT) calculations were performed with the ABINIT code version 9.11.0 [19] in the PBEsol+U framework [20] for the exchange-correlation functional and using the JTH projected augmented wave atomic potentials (v1.1) [21], including spin-orbit coupling (SOC) treatment (unless stated otherwise). A Hubbard-U correction of 4.0 eV was applied to the 3d Co shell, adjusted to match the total (spin + orbital) experimental magnetic moment of $3.33 \mu_B$ [22]. We have checked that the qualitative results are not affected by the U value (see Supplementary Material Tab. S.II.). The Kohn-Sham pseudo-wave functions were expanded over a plane-wave basis set with a kinetic energy cut-off of 24 Ha and with a cut-off for the PAW double grid kinetic energy cut-off of 48 Ha. We used a strict convergence threshold of 2.7×10^{-12} eV for the total energy on the self-consistent cycle, to determine the DMCs accurately. The BZ of the magnetic unit cell was sampled with a Monkhorst-Pack k-point grid of $6 \times 6 \times 4$ points in the G-AFM unit cell ($\sqrt{2} \times \sqrt{2} \times 2$ with respect to the crystal unit cell). We use density functional theory perturbation (DFPT) to determine the eigenvalues and eigendisplacements of phonons as well as the Born effective charges [23] to calculate the lattice contribution to the (anti-)magnetolectric response.

Above 115 K, KCoF_3 can be found in a non magnetic cubic perovskite phase described by the space group $Pm\bar{3}m$ (#192) with 5 atoms in the unit cell. Below the Néel temperature $T_N = 115 \text{ K}$ [24–26], KCoF_3 undergoes an antiferromagnetic (AFM) phase transition with an associated propagation wavevector $k = (1/2, 1/2, 1/2)$. This leads to a G-type AFM magnetic ground state, i.e. each Co magnetic moment is surrounded by Co first nearest neighbours with opposite magnetic moments. Our calculations are consistent with the experimental magnetic ground state as we found that the G-AFM phase is the most energetically favorable among the main commensurate magnetic orderings that we sampled (see Supplementary Material Table S.I.). This G-AFM ground state is also confirmed by the magnon dispersion calculated in the cubic phase [27] (see Supplementary Material Fig. S.1) where the lowest energy point in the dispersion is at the $k = (1/2, 1/2, 1/2)$ point corresponding to the G-AFM phase. Our calculated lattice parameters are in good agreement with the experimental values ($4.069 \pm$

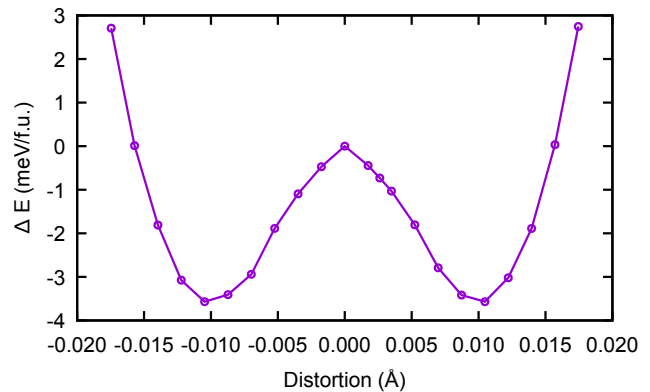


FIG. 1. Energy evolution under the first-order type Jahn-Teller rigid distortion in KCoF_3 in the G-AFM magnetic state including SOC but at fixed cell parameter (the one of the high symmetry reference, see Table S.I). The zero energy is taken from the $P14/mmm'$ high symmetry phase including SOC (Table S.I). Under the full cell relaxation, a total gain of 23.1 meV/f.u. is obtained, showing that the elastic contribution is important.

0.001 Å) [24, 28] for all considered magnetic orders, with the important mention that only the ferromagnetic phase preserves the cubic geometry (4.069 Å), while the antiferromagnetic phases promote the structure to a (slight) tetragonal geometry (see Supplementary Material Tab. S.I.).

Our calculated total magnetic moment of the Co atoms is found to be $3.43 \mu_B$ irrespective of the magnetic ordering and their associated geometry, which is in good agreement with the experimental value of $3.33 \mu_B$ [22]. This calculated magnetic moment decomposes into its spin component with a value of $2.50 \mu_B$ and into its orbital counterpart with a value of $0.93 \mu_B$. While the Co^{2+} with d^7 configuration could potentially attain a maximum magnetic moment of $3 \mu_B$ for both spin and orbital contributions, totaling $6 \mu_B$ in spherical symmetry, the local rotational symmetry can greatly reduce the free ion maximum value [29]. Besides the local symmetry, the spin-orbit coupling allows for a magnetic moment transfer from the spin to the unquenched orbital magnetic moment. The magnon-phonon interaction itself is further enhanced owing to the unquenched orbital magnetic moment [30] and a residual orbital magnetic moment can be present in the cubic crystal field [31]. High spin Co^{2+} shows a remarkable orbital moment of roughly $1 \mu_B$ in octahedral coordination, as it is the case in KCoF_3 or CoO_4X_2 ($\text{X}=\text{Cl}, \text{Br}, \text{S}, \text{Se}$) [29, 32]. Although the highest reported value of Co^{2+} to our knowledge is found in $\text{SrTi}_{0.88}\text{Co}_{0.04}\text{Nb}_{0.08}\text{O}_3$ where the total magnetic moment is $5.95 \mu_B$, close to the full spin plus orbital calculated value, $g\sqrt{J^2(J+1)} = 6.63$ [33]. Nonetheless, the orbital magnetic moment in KCoF_3 is larger than in the prototypical VI_3 ($0.59 \mu_B$) [34], Fe_3O_4 ($0.44 \mu_B$) or CrO_2 ($0.06 \mu_B$) [35].

Experimentally, the antiferromagnetic order onset be-

low 115 K is simultaneous with a lattice distortion driving KCoF_3 from a cubic phase to a tetragonal phase [24]. However, there is no experimental report of the space group nor of the atom positions below 115 K, only the cell parameters values and their tetragonal splitting are reported [24]. Some authors mention that the transition can be purely elastic [36, 37], but it is based on a more speculative theoretical analysis and not supported by any experimental works nor theoretical calculations. High spin Co d^7 orbitals in the octahedra environment should be Jahn-Teller active as the two electrons of the minority channel breaks the t_{2g} 3-fold degeneracy of the octahedral cubic crystal field [38]. This situation should correspond to the so-called first-order Jahn-Teller effect [24, 39, 40]. A previous first-principles DFT calculation report that the tetragonal phase of KCoF_3 comes from a first order Jahn-Teller instability and it is associated with the cubic R zone boundary point pattern of distortion [41]. We have checked this result at the collinear level and we indeed found (i) that the cubic phase in its G-AFM state has no unstable phonon (see Supplementary Material Fig. S.2, in agreement with Fig. 5 of Dubrovin et al. [42]) and (ii) that a sudden jump in energy is observed in the cubic phase (in the collinear calculation case, see Supplementary Material Fig. S.3) once the cubic symmetry is broken, and thus before any lattice distortion is allowed, which is a finger print of an electronic instability of the first order Jahn-Teller type [41]. The full relaxation of the cell gives the typical R zone boundary point Jahn-Teller distortion (Q^{2-} distortion [38]) with the tetragonal space group $I4/mcm$. The calculation of phonon dispersion in this relaxed lower energy phase (see Supplementary Material Fig. S.4) does not exhibit any unstable mode and if we break all symmetry operations and fully relax the crystal, the system stays in this $I4/mcm$ phase, such that we can conclude that this phase is locally stable.

In our search for local minima but including the spin-orbit coupling, we found (i) the $I4/mcm$ phase with a gain of energy of 23.1 meV/f.u. (with respect to the G-AFM high symmetry reference with spin-orbit coupling, see Fig. 1) (ii) a purely elastic distorted phase, with the space group $P2_1/c$ and reducing the energy by 0.7 meV/f.u., hence a gain of energy which is much smaller than the $I4/mcm$ phase, and (iii) another Jahn-Teller distortion phase associated with a M-point distortion (Q^{2+} distortion, $I4/mbm$ space group [38]) and lowering the energy by 11.1 meV/f.u., again higher than the $I4/mcm$ phase. Hence, according to our calculations, the G-AFM $I4/mcm$ phase is the ground state of KCoF_3 and it comes from a first-order Jahn-Teller electronic instability combined with a lattice distortion associated with the R-point distortion [38].

In our non-collinear calculation, we found that the magnetic crystal space group is $I4'/mcm'$ for a magnetic easy-axis along the lattice vector direction (here conventionally along the z direction within an unit cell of $\sqrt{2} \times \sqrt{2} \times 2$ with respect to the cubic unit cell). The only internal degree of freedom falls on the basal F atom

at the 8h Wyckoff site ($x, x + \frac{1}{2}, 0$), with $x=0.03 \text{ \AA}$. The distortion corresponds to the typical Jahn-Teller distortion from R-point [38], i.e. an in-plane stretching of the octahedra in anti-phase with both in- and out-of-plane neighbouring octahedra (see inset of Fig. 2). We would like to mention here that the cubic phase cannot stay in cubic symmetries with the G-AFM magnetic phase and the spin-orbit on. Indeed, the magnetic space group is the tetragonal $P4'/mm'm'$ (for a magnetic easy-axis along the lattice vector direction) such that the electronic instability is always relaxed. In this situation with the spin-orbit coupling on, we cannot probe the sudden jump in energy due to the electronic instability [41] as shown in Fig. 1. The energy well is closer to a smooth double well, but we can still observe a dominant linear evolution of the energy around the zero distortion.

Let us address the implication of the Jahn-Teller electronic instability on the magnetism of KCoF_3 . In Fig. 2 we show the evolution of the Co atom orbital angular momentum under the Jahn-Teller distortion. The orbital magnetic moment of Co atoms carries a large value in the cubic phase of about $0.95 \mu_B$, while it is independent on the magnetic ordering. Following the distortion pattern associated with the Jahn-Teller instability (see Supp Mat Figure S.5), we find that the orbital magnetization slowly stabilizes for values of x above 0.03 \AA to about $1/3$ of the initial value (see Fig. 2). Yet it is important to remark that the energy minimum of the $I4'/mcm'$ Jahn-Teller ground state phase is reached much earlier than the orbital magnetization stabilization for values of x around 0.01 \AA , locking the value of the orbital magnetic moment to $0.55 \mu_B$ (dotted line in Fig. 2). We can see from this analysis that the orbital magnetic moment strongly vary with respect to the Jahn-Teller pattern of atomic distortions so that we can wonder how each individual atom motion can affect the magnetic properties of KCoF_3 . Within the same regime of distortion amplitude, the spin contribution to the magnetic moment does not vary significantly (0.4%).

One way to check how individual atomic motion can affect the magnetism is through the dynamical magnetic effective charges. In Table I, we show those DMC tensorial elements. Unexpectedly for a non-multiferroic material, we found that that the DMC of K and F atoms can be non-zero by symmetry in the $I4'/mcm'$ ground state phase while it is zero for the Co atom. The K atom seats at the 4a Wyckoff position, which corresponds to the $4'22'$ magnetic point group that allows for the xx and yy DMC pseudotensor components to be non zero where $Z_{xx}^{*m} = -Z_{yy}^{*m}$. The DMC components associated with the Co atom at the 4d Wyckoff position are strictly zero by symmetry, another surprising result considering that one would expect that the magnetic atom will carry the largest DMC values [10, 12]. The apical fluorine atom at the 4b Wyckoff site is associated with the $-4'2m'$ magnetic point group, which allows the diagonal xx , yy and zz DMC components to be non zero and where $Z_{xx}^{*m} = Z_{yy}^{*m} \neq Z_{zz}^{*m}$. At last, the basal fluorine

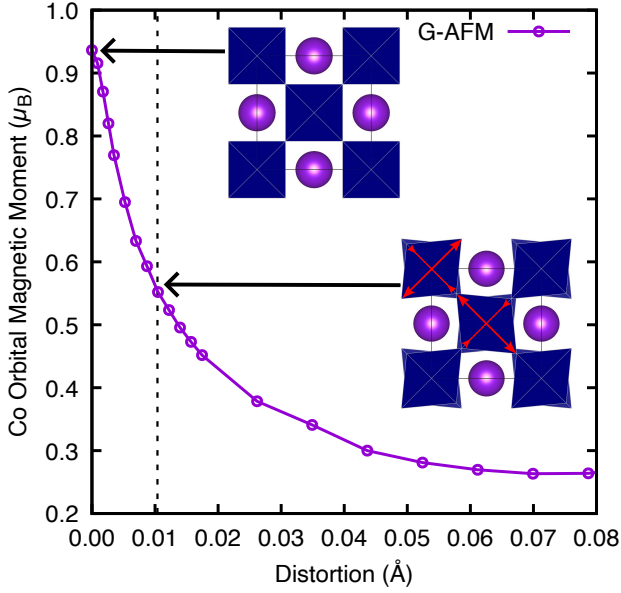


FIG. 2. Evolution of Co orbital magnetic moment with respect to the Jahn-Teller distortion amplitude.

is located at the 8h Wyckoff position where only the yz and zy off-diagonal DMC elements are non zero and with $Z_{yz}^{*m} \neq Z_{zy}^{*m}$.

Let us now check how large are those DMC from DFT calculations. We report our calculated DMC by finite differences for each atom in the last two columns of Tab. I by splitting the spin (\vec{S}) and orbital (\vec{L}) contributions. We first note that those two contributions are roughly on par for all atoms. For K atom, we obtain a spin contribution of $-54 \times 10^{-2} \mu_B/\text{\AA}$ and an orbital one of $-62 \times 10^{-2} \mu_B/\text{\AA}$. Those values are rather large as they give a total of $116 \times 10^{-2} \mu_B/\text{\AA}$, which is larger than all the previous reports, such as BiCoO_3 with about $30 \times 10^{-2} \mu_B/\text{\AA}$ [12] or Cr_2O_3 with about $6 \times 10^{-2} \mu_B/\text{\AA}$, beside the fictitious KITPite case [10]. Looking at F_{api} atom, we found even larger values of $90 \times 10^{-2} \mu_B/\text{\AA}$ and $96 \times 10^{-2} \mu_B/\text{\AA}$ for the spin and orbital contributions of the xx/yy tensor component respectively, which makes a total of $186 \times 10^{-2} \mu_B/\text{\AA}$. This is the largest DMC values up-to-date in a real material, and it is almost as large as those reported for the fictitious KITPite [10]. The Z_{zz}^{*m} component is also non zero but has a negligible spin contribution (lower than the calculations' precision) and an orbital contribution of $-10 \times 10^{-2} \mu_B/\text{\AA}$. The zz DMC component of F_{api} is then almost entirely due to the orbital contribution. The Z_{yz}^{*m} tensor component of the F_{bas} atom also gives a sizeable value of $42 \times 10^{-2} \mu_B/\text{\AA}$ and $34 \times 10^{-2} \mu_B/\text{\AA}$ for the spin and orbital contributions respectively, hence giving a total of $76 \times 10^{-2} \mu_B/\text{\AA}$. The value of Z_{zy}^{*m} of F_{bas} is found to be lower than the precision of our calculations.

The magnetic space group of the ground state phase of KCoF_3 with the magnetic moment along the z direction is $I4'/mcm'$, which does not allow for a magnetoelectric response. However, as the magnetic effec-

TABLE I. DMC tensor elements of each inequivalent atoms in the $I4'/mcm'$ phase of KCoF_3 based on the symmetry analysis. The *Symm.* column gives the magnetic point group of the Wyckoff site given in the second column and the fourth column gives the non-zero DMC tensor elements. In the last two columns, the corresponding calculated values for both spin (\vec{S}) and orbital (\vec{L}) contributions are given in $10^{-2} \mu_B/\text{\AA}$.

Atom	Wyc.	Symm.	non-zero components	\vec{S}	\vec{L}
K	4a	$4'22'$	$Z_{xx}^{*m} = -Z_{yy}^{*m}$	-54	-62
Co	4d	$m'mm'$	-	-	-
F_{api}	4b	$-4'2m'$	$Z_{xx}^{*m} = Z_{yy}^{*m}, Z_{zz}^{*m}$	$90, < 3$	$96, -10$
F_{bas}	8h	$m'm2'$	Z_{yz}^{*m}, Z_{zy}^{*m}	$42, < 3$	$34, < 3$

tive charges are non-zero it means that the crystal can be anti-magnetoelectric [12]. We have found that each spin sublattice carries a total response of 105 ps/m per formula unit, i.e. 210 ps/m per spin-channel, splitted between the spin-lattice $\alpha^{\vec{S},latt} = 50 \text{ ps/m}$ and the orbital-lattice $\alpha^{\vec{L},latt} = 55 \text{ ps/m}$ contributions. Hence, the local equivalent magnetoelectric response is rather large.

To check how general is the possibility to have non zero DMCs and to have anti-magnetoelectric, we have checked from symmetry analysis if the cubic, M and R Jahn-Teller phases, R and M octahedra rotations phases and the most common $Pnma$ perovskite phase within the ferromagnetic, C-, A- and G-type AFM magnetic orders are magnetoelectric, anti-magnetoelectric or none of the two. We report these results in Tables S.III. and S.IV. of the Supplementary Material. We can directly see that none of those phases are magnetoelectric and that all of the phases are anti-magnetoelectric beside the ferromagnetic cubic cases. From this reduced analysis we can see that the anti-magnetoelectric property is actually a very common property of perovskites and this is probably the case for all crystals.

In summary, we have studied the anti-magnetoelectric properties and the DMCs of KCoF_3 in the context of a first-order tetragonal Jahn-Teller distortion. We found that the DMCs of Co are zero and that the ones of K and F atoms are very large, the largest value being reached by the apical fluorine anion when moving it along the x or y direction perpendicular to the tetragonal axis. All of the large values are evenly split between spin and orbital magnetization, which sum to make giant values, the largest ever reported by far in real materials. We could demonstrate from symmetry arguments the shape of the DMC tensors of each atom and that the DMC of Co cation should indeed be zero, even though it is the source of magnetism in KCoF_3 crystal. The presence of a Jahn-Teller orbital ordering as it is the case in KCoF_3 seems to be an important condition to obtain large DMC, however, this would require a more systematic and deeper analysis, which is beyond the scope of the present paper. We could also show from symmetry arguments that the anti-magnetoelectric response is present in numerous non-functional phases of perovskites and that it could

be a more general property of magnetic materials that goes beyond the cases of multiferroic or magnetoelectric crystals. We hope that our works will encourage further studies of how the DMC could be an important property of materials.

The authors acknowledges the FNRS and the Excellence of Science program (EOS “ShapeME”, No. 40007525) funded by the FWO and F.R.S.-FNRS. Computational resources have been provided by the Con-

sortium des Équipements de Calcul Intensif (CÉCI), funded by the Fonds de la Recherche Scientifique (F.R.S.-FNRS) under Grant No. 2.5020.11 and the Tier-1 Lucia supercomputer of the Walloon Region, infrastructure funded by the Walloon Region under the grant agreement n°1910247 and by the High Performance Computing Mesocenter of the University of Lille financed by the University, the Hauts-de-France Region, the State, the FEDER and the University’s laboratories through a pooling process.

-
- [1] N. A. Spaldin and R. Ramesh, *Nature Materials* **18**, 203 (2019).
- [2] M. Fiebig, T. Lottermoser, D. Meier, and M. Trassin, *Nature Reviews Materials* **1**, 16046 (2016).
- [3] G. Nénert, in *Photonic and Electronic Properties of Fluoride Materials*, edited by A. Tressaud and K. Poepelmeier (Elsevier, Boston, 2016) pp. 383–398.
- [4] M. Fiebig, *Journal of Physics D: Applied Physics* **38**, R123 (2005).
- [5] L. Schaufelberger, M. E. Merkel, A. M. Tehrani, N. A. Spaldin, and C. Ederer, *Phys. Rev. Res.* **5**, 033172 (2023).
- [6] F. Thöle and N. A. Spaldin, *Philosophical Transactions of the Royal Society A: Mathematical, Physical and Engineering Sciences* **376**, 20170450 (2018).
- [7] F. Thöle, A. Keliri, and N. A. Spaldin, *Journal of Applied Physics* **127**, 213905 (2020).
- [8] A. Urru and N. A. Spaldin, *Annals of Physics* **447**, 168964 (2022).
- [9] X. H. Verbeek, A. Urru, and N. A. Spaldin, *Physical Review Research* **5**, L042018 (2023).
- [10] M. Ye and D. Vanderbilt, *Physical Review B* **89**, 064301 (2014).
- [11] A. Scaramucci, E. Bousquet, M. Fechner, M. Mostovoy, and N. A. Spaldin, *Phys. Rev. Lett.* **109**, 197203 (2012).
- [12] M. Braun, B. Guster, A. Urru, H. Kabbour, and E. Bousquet, *Large dynamical magnetic effective charges and anti-magnetoelectricity from spin and orbital origin in multiferroic bico₃* (2024), arXiv:2406.06298 [cond-mat.mtrl-sci].
- [13] D. Go, D. Jo, H.-W. Lee, M. Kläui, and Y. Mokrousov, *Europhysics Letters* **135**, 37001 (2021).
- [14] S. Manipatruni, D. E. Nikonov, C.-C. Lin, T. A. Gosavi, H. Liu, B. Prasad, Y.-L. Huang, E. Bonturim, R. Ramesh, and I. A. Young, *Nature* **565**, 35 (2019).
- [15] E. Bousquet and N. Spaldin, *Physical Review Letters* **107**, 197603 (2011).
- [16] J. Íñiguez, *Phys. Rev. Lett.* **101**, 117201 (2008).
- [17] A. Malashevich, S. Coh, I. Souza, and D. Vanderbilt, *Physical Review B* **86**, 094430 (2012).
- [18] I. V. Solovyev and T. V. Kolodiazhnyi, *Physical Review B* **94**, 094427 (2016).
- [19] X. Gonze et al., *Computer Physics Communications* **248**, 107042 (2020).
- [20] M. Torrent, F. Jollet, F. Bottin, G. Zerah, and X. Gonze, *Computational Materials Science* **42**, 337 (2008).
- [21] F. Jollet, M. Torrent, and N. Holzwarth, *Computer Physics Communications* **185**, 1246 (2014).
- [22] V. Scatturin, L. Corliss, N. Elliott, and J. Hastings, *Acta Crystallographica* **14**, 19 (1961).
- [23] X. Gonze and C. Lee, *Physical Review B* **55**, 10355 (1997).
- [24] A. Okazaki and Y. Suemune, *Journal of the Physical Society of Japan* **16**, 671 (1961).
- [25] K. Hirakawa, K. Hirakawa, and T. Hashimoto, *Journal of the Physical Society of Japan* **15**, 2063 (1960).
- [26] A. Oleaga, A. Salazar, and D. Skrzypek, *Journal of Alloys and Compounds* **629**, 178 (2015).
- [27] X. He, N. Helbig, M. J. Verstraete, and E. Bousquet, *Computer Physics Communications* **264**, 107938 (2021), arXiv:2009.01910 [cond-mat.mtrl-sci].
- [28] S. Wang, W. Li, G. Wang, D. Dong, J. Shi, X. Li, P. Li, and W. Tang, *Powder Diffraction* **28**, S3–S6 (2013).
- [29] H.-J. Koo, R. K. Kremer, and M.-H. Whangbo, *Inorganic Chemistry* **59**, 18319 (2020), pMID: 33289382.
- [30] T. Isu and K. Motizuki, *Journal of the Physical Society of Japan* **45**, 806 (1978).
- [31] J. Kanamori, *Progress of Theoretical Physics* **17**, 177 (1957).
- [32] M.-H. Whangbo, R. K. Kremer, and H.-J. Koo, *The Journal of Physical Chemistry C* **126**, 16563 (2022).
- [33] Y. M. Oey and R. Cava, *Materials Research Bulletin* **122**, 110667 (2020).
- [34] D. Hovančík, J. Pospíšil, K. Carva, V. Sechovský, and C. Piamonteze, *Nano Letters* **23**, 1175 (2023).
- [35] D. Huang, C. Chang, J. Chen, H.-J. Lin, S. Chung, H.-T. Jeng, G. Guo, W. Wu, S. Shyu, and C. Chen, *Journal of Electron Spectroscopy and Related Phenomena* **137-140**, 633 (2004), iCESS-9 Proceedings of the 9th International Conference on Electronic Spectroscopy and Structure.
- [36] J. Kanamori, *Journal of Applied Physics* **31**, S14 (1960).
- [37] J. F. Scott, *Rev. Mod. Phys.* **46**, 83 (1974).
- [38] M. M. Schmitt, Y. Zhang, A. Mercy, and P. Ghosez, *Phys. Rev. B* **101**, 214304 (2020).
- [39] K. I. Kugel’ and D. I. Khomskii, *Soviet Physics Uspekhi* **25**, 231 (1982).
- [40] I. B. Bersuker, ed., *The Jahn-Teller Effect and Vibronic Interactions in Modern Chemistry* (Springer New York, NY, 1984).
- [41] J. Varignon, M. Bibes, and A. Zunger, *Phys. Rev. Res.* **1**, 033131 (2019).
- [42] R. M. Dubrovin, A. C. Garcia-Castro, N. V. Siverin, N. N. Novikova, K. N. Boldyrev, A. H. Romero, and R. V. Pisarev, *Phys. Rev. B* **104**, 144304 (2021).

Supplementary Material: Large dynamical magnetic effective charges in the Jahn-Teller KCoF_3

Bogdan Guster,¹ Maxime Braun,^{1,2} and Eric Bousquet¹

¹*Physique Théorique des Matériaux, QMAT, CESAM, Université de Liège, B-4000 Sart-Tilman, Belgium*

²*Univ. Lille, CNRS, Centrale Lille, ENSCL, Univ. Artois, UMR 8181-UCCS-Unité de Catalyse et Chimie du Solide, F-59000 Lille, France*

I. SUPPLEMENTARY TABLES

TABLE S.I. Energy and lattice parameters of the common commensurate magnetic phases in high symmetry KCoF_3 , along with the associated magnetic space groups. We can see that the magnetic ordering breaks the cubic symmetry when considering magnetic moment orientation with spin-orbit coupling in the calculation.

Magnetic Phase	E (meV/f.u.)	a(Å)	c(Å)	Mag. S.G.
G-AFM	0	4.0703	3.9978	$P14/mmm'$
C-AFM	28	4.0707	4.0074	$P2c4/mmm'$
A-AFM	47	4.0790	4.0008	$Pp4'/mmm'$
FM	84	4.0690	-	$P4/mmm'$

TABLE S.II. Relative energy difference (ΔE) between the cubic and the Jahn-Teller and the elastic phase with respect to the Hubbard U value. The corresponding lattice parameters of each case is listed as well. All lengths are expressed in Bohr.

#	Cubic			JT - Q^{2-}				Monoclinic			
	a	b	c	a	b	c	ΔE (meV/f.u.)	a	b	c	ΔE (meV/f.u.)
U								α	β	γ	
4.0	10.695	10.695	15.658	10.880	10.880	15.124	-23.1	10.885	10.885	15.123	-0.7
								90	90	88.00	
4.5	10.696	10.696	15.658	10.887	10.887	15.137	-22.1	10.887	10.892	15.133	-0.7
								90	90	88.03	
5.0	10.709	10.709	15.658	10.890	10.890	15.130	-21.1	10.893	10.897	15.137	-0.7
								90	90	88.05	
6.0	10.719	10.719	15.663	10.898	10.898	15.158	-19.5	10.899	10.901	15.163	-0.7
								90	90	88.15	
8.0	10.727	10.727	15.667	10.910	10.910	15.206	-17.2	10.915	10.911	15.191	-1.1
								90	90	88.21	
10.0	10.765	10.765	15.677	10.923	10.923	15.232	-14.8	10.926	10.928	15.224	-0.7
								90	90	88.33	

TABLE S.III. Magnetic space groups of KCoF_3 in different magnetic configurations. All listed magnetic space groups are antiferromagnetic (A) except for cubic FM that are neither ME nor Anti-ME (\emptyset).

Geometry	Mag. Phase	Easy axis	Mag. Point Group	Mag. Space group	ME
Cubic	FM	x,y,z	$4/\text{mm}'\text{m}'$	123.345	\emptyset
		xy,xz,yz	$\text{m}'\text{m}'\text{m}'$	65.486	\emptyset
		xyz	$-\text{3m}'$	166.101	\emptyset
	C-AFM	x,y	$\text{mmm}.1'$	67.509	A
		z	$4/\text{mmm}.1'$	127.397	A
		xy	$\text{mmm}.1'$	53.334	A
		xz,yz	$2/\text{m}.1'$	12.64	A
		xyz	$2/\text{m}.1'$	14.83	A
		x,y	$\text{mmm}.1'$	51.298	A
	A-AFM	z	$4/\text{mmm}.1'$	124.360	A
		xy	$\text{mmm}.1'$	63.466	A
		xz,yz	$2/\text{m}.1'$	13.72	A
		xyz	$2/\text{m}.1'$	15.90	A
	G-AFM	x,y,z	$4/\text{mmm}.1'$	140.550	A
		xy,xz,yz	$\text{mmm}.1'$	74.562	A
xyz		$-\text{3m}.1'$	167.108	A	
R-JT	FM	z	$4/\text{mm}'\text{m}'$	140.547	A
		x,y	$\text{m}'\text{m}'\text{m}'$	69.524	A
	C-AFM	z	$4/\text{mmm}.1'$	135.494	A
		x,y	$\text{mmm}.1'$	64.480	A
	A-AFM	z	$4/\text{mmm}.1'$	124.362	A
		x,y	$\text{mmm}.1'$	64.480	A
G-AFM	z	$4'/\text{mm}'\text{m}'$	140.545	A	
	x,y	$\text{m}'\text{m}'\text{m}'$	69.524	A	
M-JT	FM	z	$4/\text{mm}'\text{m}'$	127.393	A
		x,y	$\text{m}'\text{m}'\text{m}'$	65.486	A
	C-AFM	z	$4'/\text{mm}'\text{m}'$	127.391	A
		x,y	$\text{m}'\text{m}'\text{m}'$	65.486	A
	A-AFM	z	$4/\text{mmm}.1'$	128.408	A
		x,y	$\text{mmm}.1'$	63.466	A
G-AFM	z	$\text{mmm}.1'$	63.466	A	
	x,y	$4/\text{mmm}.1'$	135.492	A	
R-OR	FM	z	$4/\text{mm}'\text{m}'$	140.547	A
		x,y	$\text{m}'\text{m}'\text{m}'$	69.524	A
	C-AFM	z	$4/\text{mmm}.1'$	124.362	A
		x,y	$\text{mmm}.1'$	64.480	A
	A-AFM	z	$4/\text{mmm}.1'$	127.398	A
		x,y	$\text{mmm}.1'$	64.480	A
G-AFM	z	$4/\text{mmm}.1$	140.541	A	
	x,y	$\text{m}'\text{m}'\text{m}'$	69.524	A	
M-OR	FM	z	$4/\text{mm}'\text{m}'$	127.393	A
		x,y	$\text{m}'\text{m}'\text{m}'$	65.486	A
	C-AFM	z	$4/\text{mmm}.1'$	128.408	A
		x,y	$\text{mmm}.1'$	63.466	A
	A-AFM	z	$4/\text{mmm}.1$	127.387	A
		x,y	$\text{m}'\text{m}'\text{m}'$	65.486	A
G-AFM	z	$4/\text{mmm}.1'$	127.396	A	
	x,y	$\text{mmm}.1'$	63.466	A	

TABLE S.IV. Most common reported space group among perovskites (continued from Table S.III), i.e. for $Pnma$ space group. All listed magnetic space groups are anti-magnetolectric (A).

Geometry	Mag. Phase	Easy Axis	Mag.Point Group	Mag. Space Group	ME
$Pnma$	FM	x	m'm'm	62.446	A
		y	m'm'm	62.447	A
		z	m'm'm	62.448	A
	A-AFM	x	mmm	62.441	A
		y	m'm'm	62.448	A
		z	m'm'm	62.447	A
	C-AFM	x	m'm'm	62.447	A
		y	m'm'm	62.446	A
		z	mmm	62.441	A
	G-AFM	x	m'm'm	62.448	A
		y	mmm	62.441	A
		z	m'm'm	62.446	A

TABLE S.V. Calculated Born effective charges tensor components (in unit of the elemental charge e) in the FM phase of $KCoF_3$ in the cubic geometry. Columns refer to derivatives with respect to the electric field and lines to derivatives with respect to atomic positions, in atomic units.

Atom	Born Effective Charge (e)			
	$\partial/\partial\mathcal{E}_x$	$\partial/\partial\mathcal{E}_y$	$\partial/\partial\mathcal{E}_z$	
K	$\partial/\partial\tau_x$	1.19	0	0
	$\partial/\partial\tau_y$	0	1.19	0
	$\partial/\partial\tau_z$	0	0	1.21
Co	$\partial/\partial\tau_x$	2.01	0.	0
	$\partial/\partial\tau_y$	0	2.01	0
	$\partial/\partial\tau_z$	0	0	2.39
F_{api}	$\partial/\partial\tau_x$	-0.82	0	0
	$\partial/\partial\tau_y$	0	-0.82	0
	$\partial/\partial\tau_z$	0	0	-1.64
F_{bas}	$\partial/\partial\tau_x$	-0.63	0.	0
	$\partial/\partial\tau_y$	0	-1.67	0
	$\partial/\partial\tau_z$	0	0	-0.82

TABLE S.VI. Calculated Born effective charges tensor components (in unit of the elemental charge e) in the G-AFM phase of $KCoF_3$ in the R-point Jahn-Teller distorted geometry. Columns refer to derivatives with respect to the electric field and lines to derivatives with respect to atomic positions, in atomic units.

Atom	Born Effective Charge (e)			
	$\partial/\partial\mathcal{E}_x$	$\partial/\partial\mathcal{E}_y$	$\partial/\partial\mathcal{E}_z$	
K	$\partial/\partial\tau_x$	1.20	0	0
	$\partial/\partial\tau_y$	0	1.20	0
	$\partial/\partial\tau_z$	0	0	1.21
Co	$\partial/\partial\tau_x$	2.13	-0.18	0
	$\partial/\partial\tau_y$	-0.18	2.13	0
	$\partial/\partial\tau_z$	0	0	2.31
F_{api}	$\partial/\partial\tau_x$	-0.78	0	0
	$\partial/\partial\tau_y$	0	-0.78	0
	$\partial/\partial\tau_z$	0	0	-1.84
F_{bas}	$\partial/\partial\tau_x$	-1.26	0.49	0
	$\partial/\partial\tau_y$	0.49	-1.26	0
	$\partial/\partial\tau_z$	0	0	-0.83

TABLE S.VII. Mode effective charges of the polar phonon modes of KCoF₃ in the JT phase.

$\omega(\text{meV})$	Character	Mode effective charge		
		x	y	z
15	A _{2u}	0	0	2.78
15	E _u	0	-2.79	0
15	E _u	2.79	0	
21	E _u	0	-0.11	0
21	E _u	-0.11	0	0
26	A _{2u}	0	0	-3.29
27	E _u	0	-2.93	0
27	E _u	-2.93	0	0
33	E _u	-0.94	0	0
33	E _u	0	0.94	0
54	E _u	-0.001	4.081	0
54	E _u	-4.081	-0.001	0
56	A _{2u}	0	0	-4.27

TABLE S.VIII. Linear spin (\vec{S}) and orbital (\vec{L}) dynamical magnetic effective charges ($10^{-2}\mu_B/\text{\AA}$) for each nonequivalent Wyckoff sites of KCoF₃ in the Jahn-Teller phase. \mathcal{H}_i refers to the magnetic field in direction i and τ_j to the atom displacement along the direction j .

Atom	Wyckoff	\vec{S}			\vec{L}			
		$\partial/\partial\tau_x$	$\partial/\partial\tau_y$	$\partial/\partial\tau_z$	$\partial/\partial\mathcal{H}_x$	$\partial/\partial\mathcal{H}_y$	$\partial/\partial\mathcal{H}_z$	
K	4a	$\partial/\partial\tau_x$	-54	-	-	-62	-	-
		$\partial/\partial\tau_y$	-	54	-	-	62	-
		$\partial/\partial\tau_z$	-	-	-	-	-	-
Co	4d	$\partial/\partial\tau_x$	-	-	-	-	-	-
		$\partial/\partial\tau_y$	-	-	< 3	-	-	< 3
		$\partial/\partial\tau_z$	-	< 3	-	-	< 3	-
F _{api}	4b	$\partial/\partial\tau_x$	90	-	-	96	-	-
		$\partial/\partial\tau_y$	-	90	-	-	96	-
		$\partial/\partial\tau_z$	-	-	≤ -3	-	-	-10
F _{bas}	8h	$\partial/\partial\tau_x$	-	-	-	-	-	-
		$\partial/\partial\tau_y$	-	-	< 3	-	-	< 3
		$\partial/\partial\tau_z$	-	42	-	-	34	-

II. SUPPLEMENTARY FIGURES

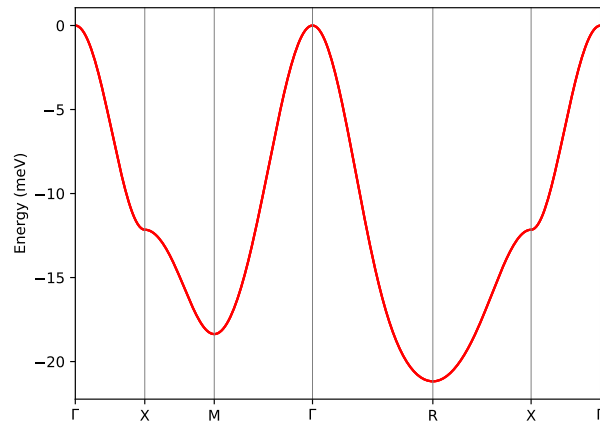


FIG. S.1. Magnon dispersion in the cubic phase of KCoF_3 in the *collinear treatment* of the FM phase, as obtained with the TB2J package [1].

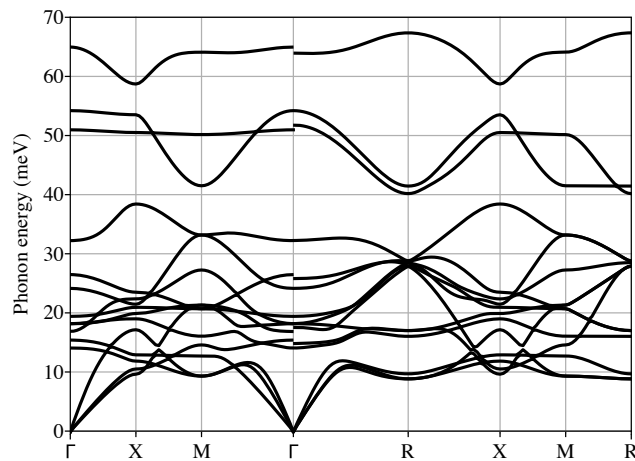


FIG. S.2. Phonon dispersion of the high-symmetry G-AFM magnetic phase of KCoF_3 , in the *collinear treatment*.

-
- [1] X. He, N. Helbig, M. J. Verstraete, and E. Bousquet, TB2J: A python package for computing magnetic interaction parameters, *Computer Physics Communications* **264**, 107938 (2021), arXiv:2009.01910 [cond-mat.mtrl-sci].
- [2] J. Varignon, M. Bibes, and A. Zunger, Origins versus fingerprints of the jahn-teller effect in d -electron abX_3 perovskites, *Phys. Rev. Res.* **1**, 033131 (2019).

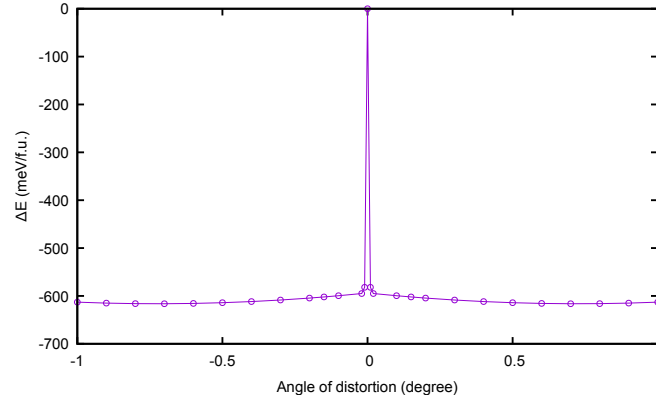


FIG. S.3. Energy evolution under the first-order type Jahn-Teller rigid distortion in KCoF₃ in the *collinear treatment* of the G-AFM magnetic state. The energy gain is comparable with the work of Varignon et al. [2] (See Fig. 7).

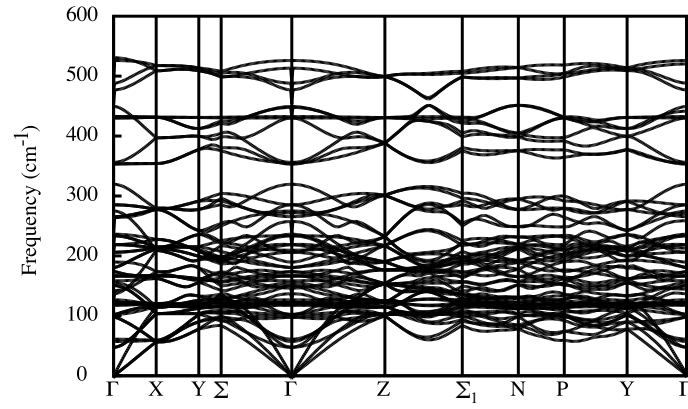


FIG. S.4. Phonon dispersion of KCoF₃ in the *collinear treatment* of the ground state G-AFM JT distorted phase.